

THE EFFECT OF MULTIPLE CRACKING ON FATIGUE CRACK GROWTH OF CURVED FUSELAGE PANELS

John G. Bakuckas, Jr.^{*}, Catherine A. Bigelow^{*}, Paul W. Tan^{*}, and Lynn Pham^{*}

Abstract: An experimental and analytical study was conducted to determine the effects of multiple cracks on the fatigue crack growth of curved fuselage panels containing one of two joint configurations: a longitudinal lap or a circumferential butt. The Full-Scale Aircraft Structural Test Evaluation and Research (FASTER) facility was used to test the two joint configurations. Fatigue crack formation and growth were monitored and recorded in real time using the Remote Controlled Crack Monitoring (RCCM) system. Geometric nonlinear finite element analyses were conducted to determine strain distributions and fracture parameters governing crack formation and growth. Comparisons with strain gage data verified the finite element models. For fatigue crack growth predictions, mixed mode stress-intensity factors were calculated using the Modified Crack Closure Integral (MCCI) method. In general, symmetric, collinear crack propagation was observed for the four panels tested. Reasonable agreement was obtained between experimental fatigue crack growth data and predictions relying on the Mode I stress-intensity factors calculated using finite element analyses of the test panels. The number of cycles to grow a fatigue crack to a predetermined length was reduced by approximately 37% due to the presence of multiple cracks for the longitudinal lap joint panels and by 27% for the circumferential butt joint panels.

INTRODUCTION

In support of the Federal Aviation Administration's (FAA) National Aging Aircraft Research Program (NAARP), experimental and analytical methodologies have been developed to assess multiple-cracking scenarios in aircraft fuselage structures. As part of this effort, a unique, state-of-the-art Full-Scale Aircraft Structural Test Evaluation and Research (FASTER) facility was developed at the FAA William J. Hughes Technical Center for testing large curved panels representative of aircraft fuselage structure. The facility is designed to simulate the actual loads an aircraft fuselage structure is subjected to while in flight, including differential pressure, longitudinal load, hoop load in the skin and frames, and shear load. Both quasi-static and long-term durability spectrum loadings can be applied in the FASTER facility. A key component of the FASTER facility is the Remote Controlled Crack Monitoring (RCCM) system developed to track and record the formation and growth of multiple cracks in real time during a test.

The current test program is part of an effort to determine the effects of multiple cracking on the fatigue crack growth and residual strength of curved fuselage structures. The curved panels used in the test program are similar to typical narrow-body fuselage

^{*} AAR-400, Airworthiness Assurance Research and Development Branch, FAA William J. Hughes Technical Center, Atlantic City International Airport, NJ 08405, USA.

structures consisting of skin, frames, shear clips, stringers, and either longitudinal splice or circumferential joints. A total of four panels were tested, two panels with a longitudinal lap splice and two with a circumferential butt joint. For each joint configuration, one panel contained a lead crack only and the other contained a lead crack with multiple cracks.

In this paper, experimental and analytical results will be presented for both joint configurations examining the effects of the multiple cracks on the fatigue crack growth. For each joint configuration, the initial damage scenario was a two-bay lead crack with and without smaller collinear multiple cracks located in the outer critical rivet row of the joint. First, a strain survey was conducted under quasi-static loading conditions on each panel to verify proper load transfer from the load application points to the test section of the panel. Comparison with an independent full-scale test on an aft fuselage section of an actual aircraft with similar structural details to the panels tested in this program confirmed appropriate applied load conditions. Fatigue crack formation and growth of the lead crack and the multiple cracks were monitored and recorded in real time using the RCCM system. To support the tests, geometric nonlinear finite element analyses were conducted. The strain distributions and fracture parameters governing crack formation and growth were determined. Comparisons with strain gage data verified the finite element models. For fatigue crack growth predictions, the mixed mode stress-intensity factors were calculated using the Modified Crack Closure Integral (MCCI) method. In the following sections, a brief description of the FASTER test fixture along with representative experimental and analytical results are presented, including strain distributions, damage growth process, and crack growth characteristics.

FULL-SCALE AIRCRAFT STRUCTURAL TEST EVALUATION AND RESEARCH (FASTER) FACILITY

The FASTER test fixture, shown in Figure 1, combines mechanical, fluid, and electronic components to apply internal pressure, longitudinal, hoop, frame, and shear loads (shear load was not used in current program) to a curved panel. As shown in the exploded view in Figure 1, the fixture consists of a base structure, a hoop load assembly, a longitudinal load assembly, a pressure box, a frame load assembly, and a shear fixture assembly. The FASTER facility also includes a computerized instrument control and data acquisition system and a remote control crack monitoring (RCCM) system not shown in Figure 1. A full description of the FASTER facility is provided in references 1-3. A brief description is provided herein.

Curved panels attach to the pressure box using an elastomeric seal. Internal pressure is applied to the panel using air or water. Mechanical loading mechanisms consisting of water actuators, load cells, and whiffle tree assemblies with a lever arm configuration are used to apply the hoop and longitudinal loads around the perimeter of the test panel. Hoop forces are applied by individual loading linkages using a two-tier, coaxial whiffle tree assembly, which generates four equal forces from each lever arm. Seven lever arms or load points are used on each side of the specimen for a total of 28 attachment points. Longitudinal forces are applied using similar loading devices on each end of the panel; 4 load points and 16 attachment points are used on each end. Hoop loads are applied at each end of each frame using a similar loading mechanism.

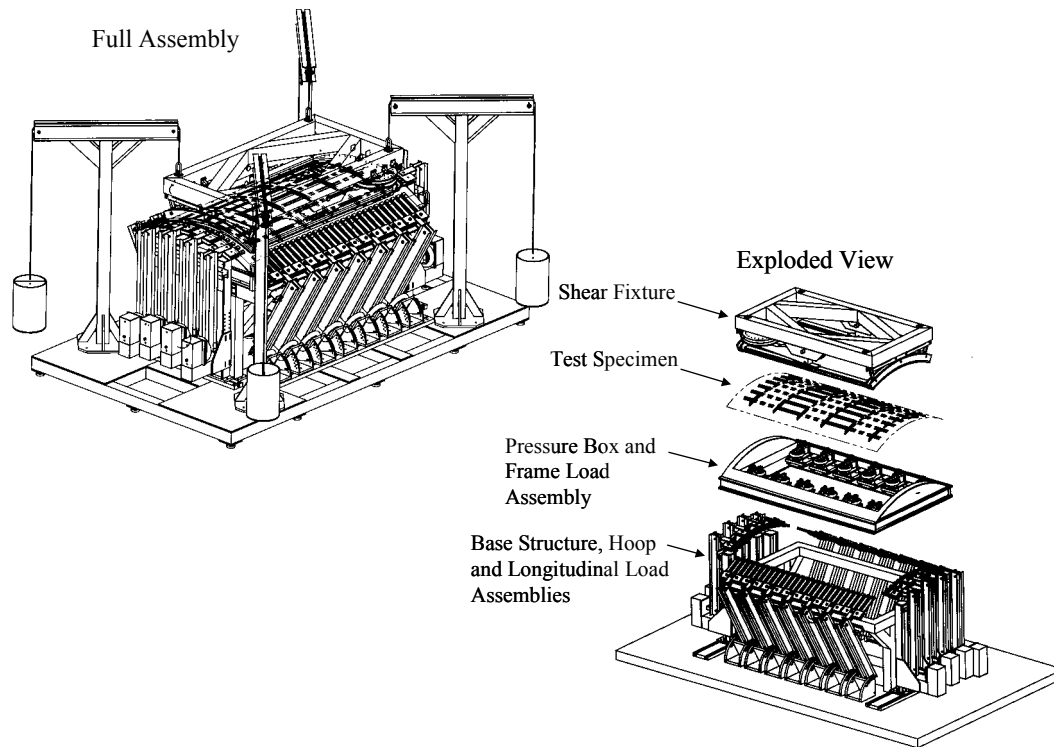


Figure 1. Full-Scale Aircraft Structural Test Evaluation and Research (FASTER) fixture

All forces are generated using water or air. The external loads are generated by applying water pressure to water actuators, which are controlled by pressure-activated dome valves. The dome valves are automatically controlled by electro-pneumatic (E/P) control valves. The E/P valves are driven by a computer control system in a closed-loop configuration using the feedback from the load cells. The operator can control the loads, speed, and type of test. Pressurization cycle can be applied at a rate of 0.2 Hz. Data from strain transducers, load transducers, pressure transducers, etc., are displayed on color monitors in real time and stored for subsequent analysis.

The Remote Controlled Crack Monitoring (RCCM) system was developed to track and record multiple crack formation and propagation during loading in real time. The RCCM system is a stand alone, computer-based video data acquisition system capable of monitoring the entire fuselage panel test surface at several levels of magnification with a field of view ranging from 0.05" up to 14". The system consists of cameras mounted to two, high-precision translation stages which are computer controlled and provide accurate and repeatable length measurements. Video data acquisition and reduction software provides real-time crack length measurement capabilities. Up to 360 of the 768 by 493 pixel digital images can be captured continuously and stored in bitmap format at a rate up to 30 frames per second. The software can playback the stored images. In addition, direct hookup to monitors and video control recording (VCR) equipment is provided for continuous real-time monitoring and recording.

EXPERIMENTAL PROCEDURE

Four panels were tested in this study: (1) panel CVP1 contains a longitudinal lap splice with a lead crack; (2) panel CVP2 has the same configuration and lead crack as CVP1

with the addition of multiple, small cracks emanating from rivet holes ahead of the lead crack; (3) panel CVP3 has a circumferential butt joint with a lead crack; and (4) panel CVP4 has the same configuration and lead crack as panel CVP3, with the addition of multiple, small cracks emanating from rivet holes ahead of the lead crack. The panels were subjected to a sequence of two loadings: (1) initial monotonic quasi-static loading to a predetermined load level; and (2) a constant amplitude cyclic loading.

Panel Configurations

The panel configuration represents a generic fuselage structure from a narrow-body aircraft fabricated according to original equipment manufacturing (OEM) specifications. For further details on the panels, see reference 3.

The panel dimensions were 120" in the longitudinal direction, 68" in the circumferential direction, with a radius of 66". Figure 2 shows the configuration for panels CVP1 and CVP2. Each panel had six frames with a 19" spacing and seven stringers with a 7.5" spacing. The Z-shaped frames and L-shaped shear clips were 7075-T6 aluminum with thicknesses of 0.071" and 0.063", respectively. The hat-shaped stringers were 7075-T6 aluminum with a thickness of 0.063", except for stringer S4 which had a thickness of 0.071".

Longitudinal Lap Joint Panel Configuration

Figure 2 shows a schematic of the longitudinal lap joint test panels, CVP1 and CVP2, including the dimensions and location of the strain gages. Photographs of panel CVP1

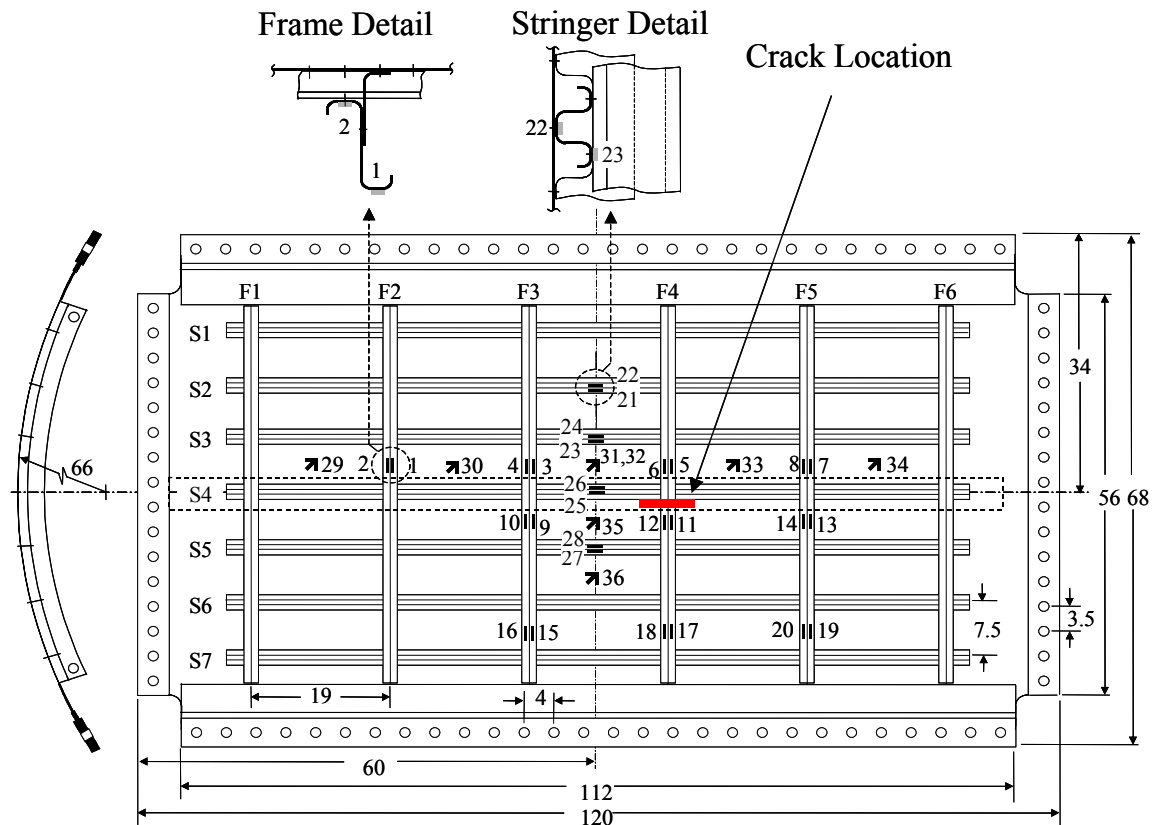


Figure 2. CVP1 and CVP2 panel configuration and strain gage locations

are shown in Figure 3. A longitudinal lap joint was located along stringer S4 as shown in Figure 4. The joint consisted of two layers of the 2024-T3 panel skin with a thickness of 0.063" and two layers of 2024-T3 finger doublers with a thickness of 0.025". Four rows of fasteners, A, B, C, and D, were used to connect the skin and doublers.

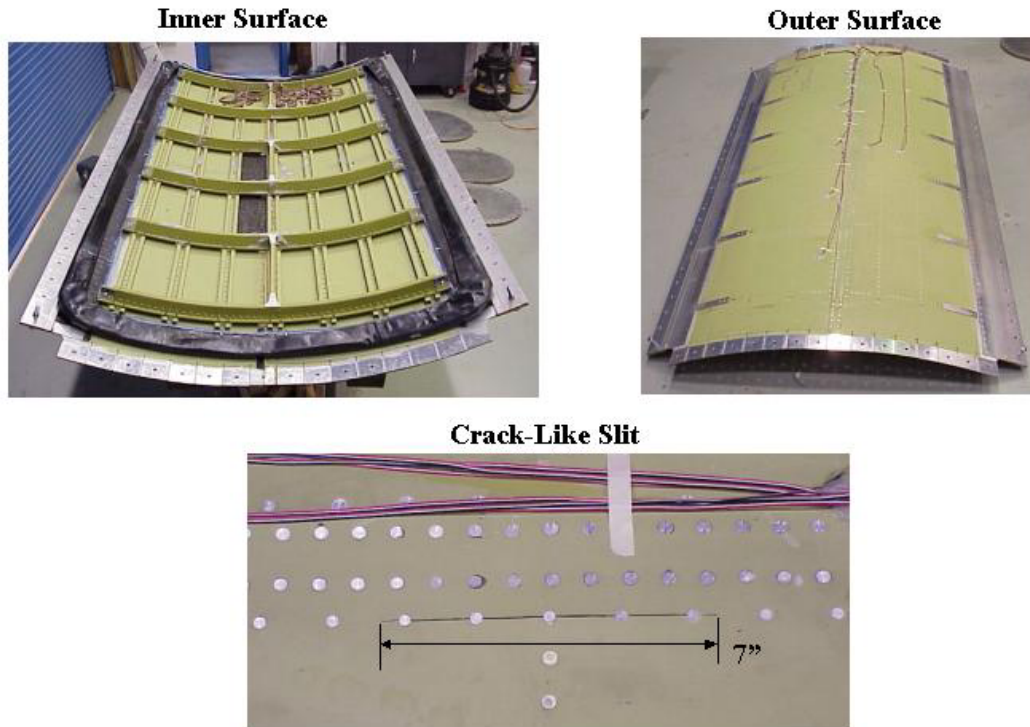


Figure 3. Photographs of panel CVP1

To determine the strain distribution, the panel was instrumented with 8 strain gage rosettes (45°) and 28 axial strain gages. The locations of the strain gages on the skin, frames, and stringers are shown in Figure 2. Twenty axial strain gages were located on both the inner and outer flanges of the frames. The stringers were instrumented with eight axial strain gages on the flange and hat section (see detail in Figure 2). The skin was instrumented with eight strain gage rosettes. At one location on the skin, two back-to-back strain gage rosettes (gages 31 and 32) were installed to provide a measure of bending of the skin.

The initial damage configuration for the two longitudinal lap joint panels is shown in Figure 4. For both panels, CVP1 and CVP2, a crack-like slit representing a lead crack was placed symmetrically across frame F4, machined in the skin along the critical rivet row A in the longitudinal lap splice. The total length of the lead crack was 7.0". Between rivet holes 2L and 2R, the crack-like slit was saw cut with a width of 0.012". The tips of the lead crack, which emanated 0.5" from the centerline of rivet holes 2L and 2R, were wire cut with a width of 0.008". For panel CVP2, small multiple cracks were machined in the first 18 rivets to the left and right of the lead crack centerline rivet. The nominal length of each crack is indicated in Figure 4. The nominal width of all the small cracks was 0.008".

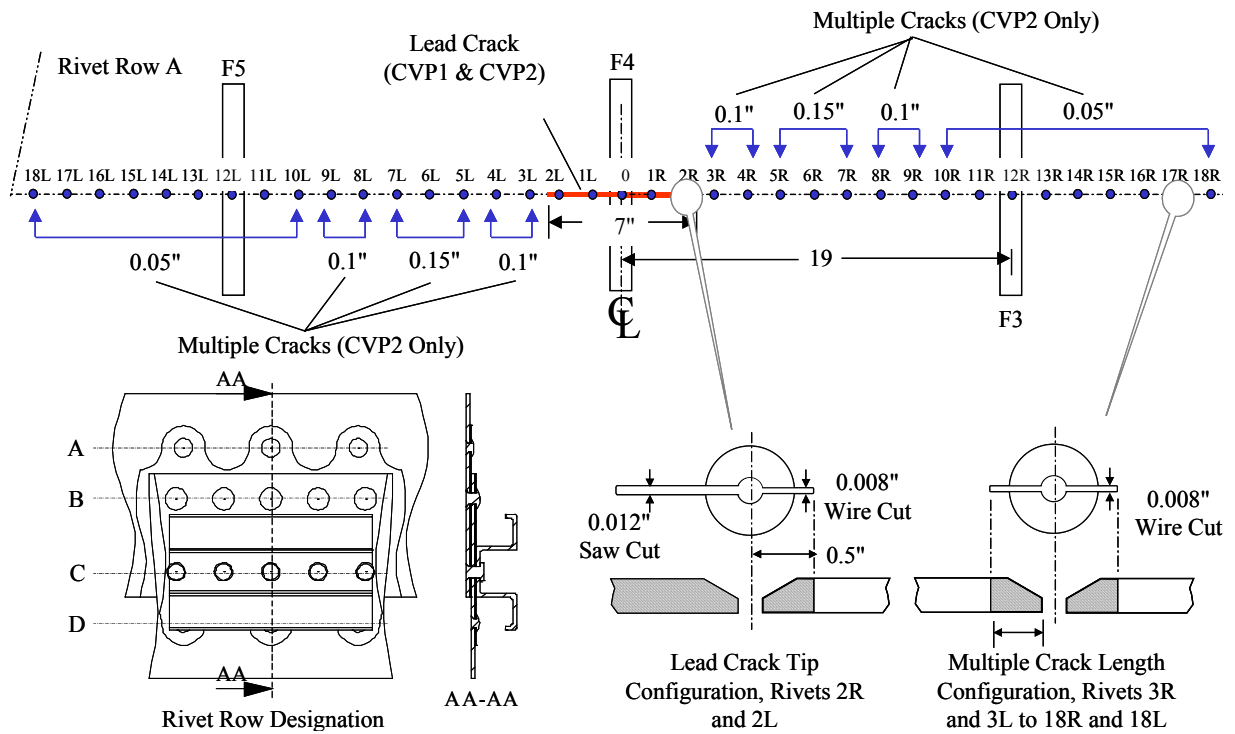


Figure 4. Joint configuration and initial damage for panels CVP1 and CVP2

Circumferential Butt Joint Panel Configuration

Figure 5 shows a schematic of the circumferential butt joint test panels, CVP3 and CVP4, including the dimensions and location of the strain gages. Both CVP3 and CVP4 test panels had a butt joint in the circumferential direction between frames F3 and F4 as shown in Figure 6. The joint consisted of two layers of the 2024-T3 panel skin with a thickness of 0.063", a 2024-T3 finger doubler with a thickness of 0.025", and a tapered doubler with

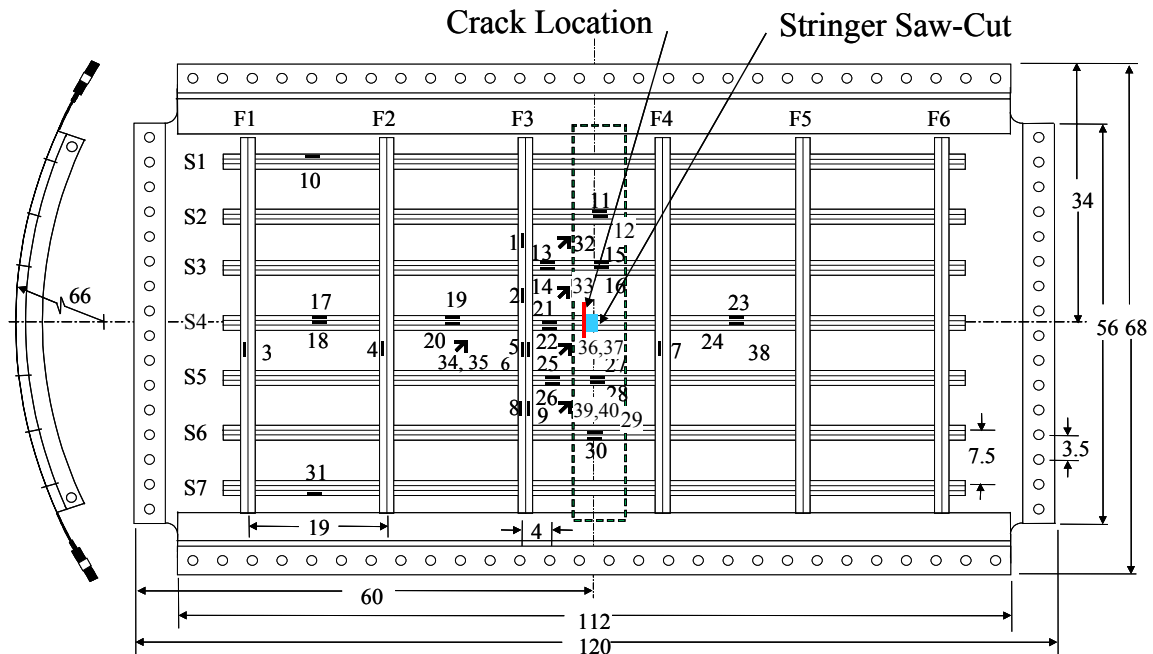


Figure 5. CVP3 and CVP4 panel configurations and strain gage locations

thickness of 0.071" which tapers to a thickness of 0.025" along the edge. Eight rows of fasteners, A through H, were used to connect the skin and doublers. Panels CVP3 and CVP4 were instrumented with 9 strain gage rosettes (45°) in the skin and 31 axial strain gages in the frames and stringers as shown in Figure 5. At two locations on the skin, at gages 36 and 37 and at gages 39 and 40, two back-to-back 45° rosette gages were installed to provide a measure of bending of the skin.

The initial damage configuration for the two circumferential lap joint panels is shown in Figure 6. For both panels, CVP3 and CVP4, a crack-like slit representing a lead crack was placed symmetrically across stringer S4, machined in the skin along the critical rivet row A in the circumferential butt joint. Stringer S4 was cut to simulate a broken stringer. The total length of the lead crack was 7.0". Between rivet holes 2L and 2R, the crack-like slit was saw cut with a width of 0.012". The tips of the lead crack, which emanated 0.5" from the centerline of rivet holes 2L and 2R, were wire cut with a width of 0.008". For panel CVP4, small multiple cracks were machined in the first 12 rivets to the left and right of the lead crack centerline rivet. The nominal length of each crack is indicated in Figure 6. The nominal width of all the small cracks was 0.008".

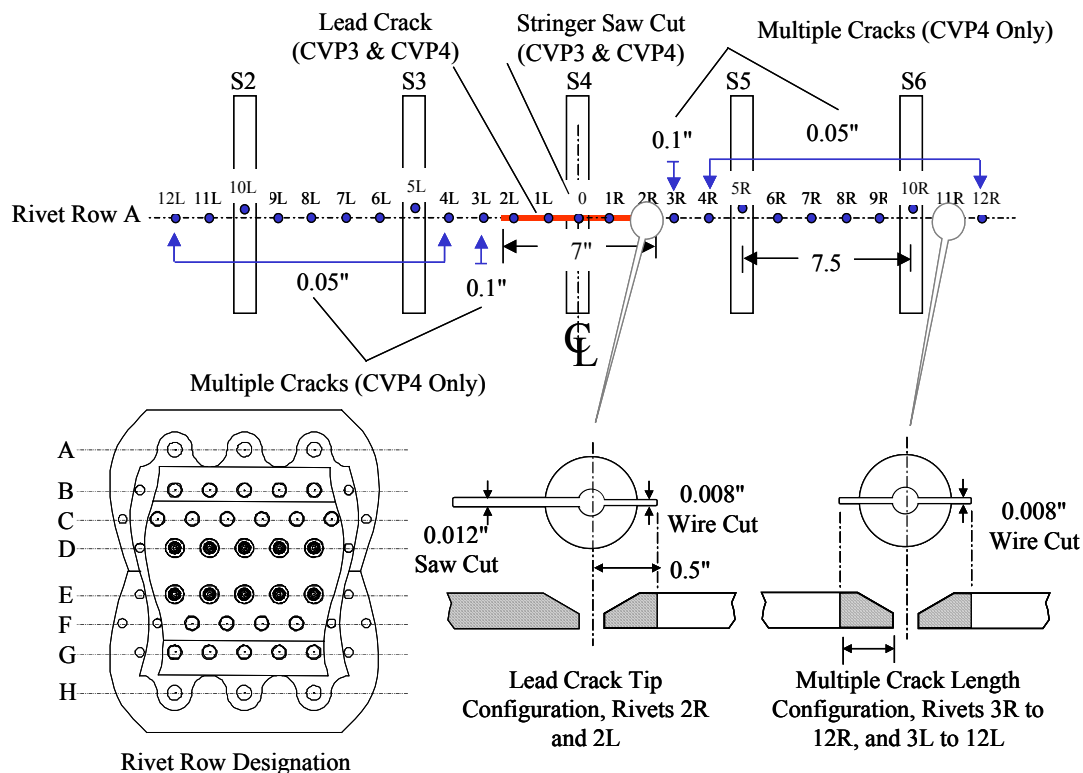


Figure 6. Joint configuration and initial damage for panels CVP3 and CVP4

Test Conditions

The longitudinal lap joint and circumferential butt joint panels were subjected to the applied loadings listed in Table 1. For the longitudinal lap joint panels, CVP1 and CVP2, the applied load simulates the cylindrical pressurization that a section of an aircraft fuselage along the neutral axis would experience. For the circumferential butt joint panels, CVP3 and CVP4, the applied load simulates a fuselage down-bending condition

Table 1. Maximum load components

Panel	Maximum Load			
	Pressure (psi)	Hoop (lb/in)	Frame (lb/in)	Long.(lb/in)
CVP1	10.1	554.6	111.9	333.3
CVP2	10.1	554.6	111.9	333.3
CVP3	8.8	483.2	97.6	875.7
CVP4	8.8	483.2	97.6	875.7

that an aircraft fuselage section along the crown of the aircraft would experience, where the longitudinal stress is 50% higher than the hoop stress.

For the strain survey test, quasi-static loadings were applied in ten equal increments up to the maximum loads listed in Table 1 for the four panels. For the fatigue crack growth test, constant amplitude loading was applied at a frequency of 0.2 Hz with an R-ratio (minimum to maximum load) of 0.1 where the maximum loads are listed in Table 1. Crack growth of the lead crack and small multiple cracks was continuously monitored and recorded using the RCCM system.

Verification Testing

To verify test results generated using the FASTER facility, comparisons were made with results from a full-scale test conducted on an aft fuselage section from a narrow-body aircraft. The aft fuselage section was mounted on a strong back fixture and pressurized quasi-statically from 0 to 7.8 psi for three tests. Strains in a section of the test article, which was similar to the panels in this test program, were compared with the strains measured at similar locations in the longitudinal lap joint panels, CVP1 and CVP2.

ANALYSIS

Geometric nonlinear finite element analyses were conducted using the commercial finite element code ABAQUS 5.8 [4]. Two analyses were conducted for each panel: the first to predict the strain distributions and the second to compute the stress-intensity factor (SIF) solutions. The SIF solutions were used to predict the fatigue crack growth characteristics of the curved panels and the predictions were compared with test results.

Description of Models

The panels were modeled using shell elements with each node having six degrees of freedom. Figure 7 shows the global view of a typical finite element model of panel CVP3. Four-noded shell elements were used throughout to model the skin, frames, shear clip, stringers, and intercostals except near the crack tips. In the immediate vicinity of the crack tips, eight-noded shell elements were used. The model contained the major geometric details and dimensions of the panels, including the cross-section properties of the substructure (frames, stringers shear-clip, intercostals), the finger doublers, and the load attachment doublers. To simplify the global panel modeling, the rivet holes were not modeled. Beam elements were used to model the rivets. The semiempirical equation developed by Swift [5], shown below, was used to calculate the shear stiffness of the beams as:

$$k_{shear} = \frac{E'd}{5 + 0.8 \left(\frac{d}{t_1} + \frac{d}{t_2} \right)} \quad (1)$$

where $E' = 10.5 \times 10^6$ psi is the effective modulus, $d = 0.1875$ " is the fastener diameter, and $t_1 = 0.063$ " and $t_2 = 0.063$ " are the thickness of the skin and substructure (shear clip or stringer), respectively. Typically, the panel models had 250,000 degrees of freedom.

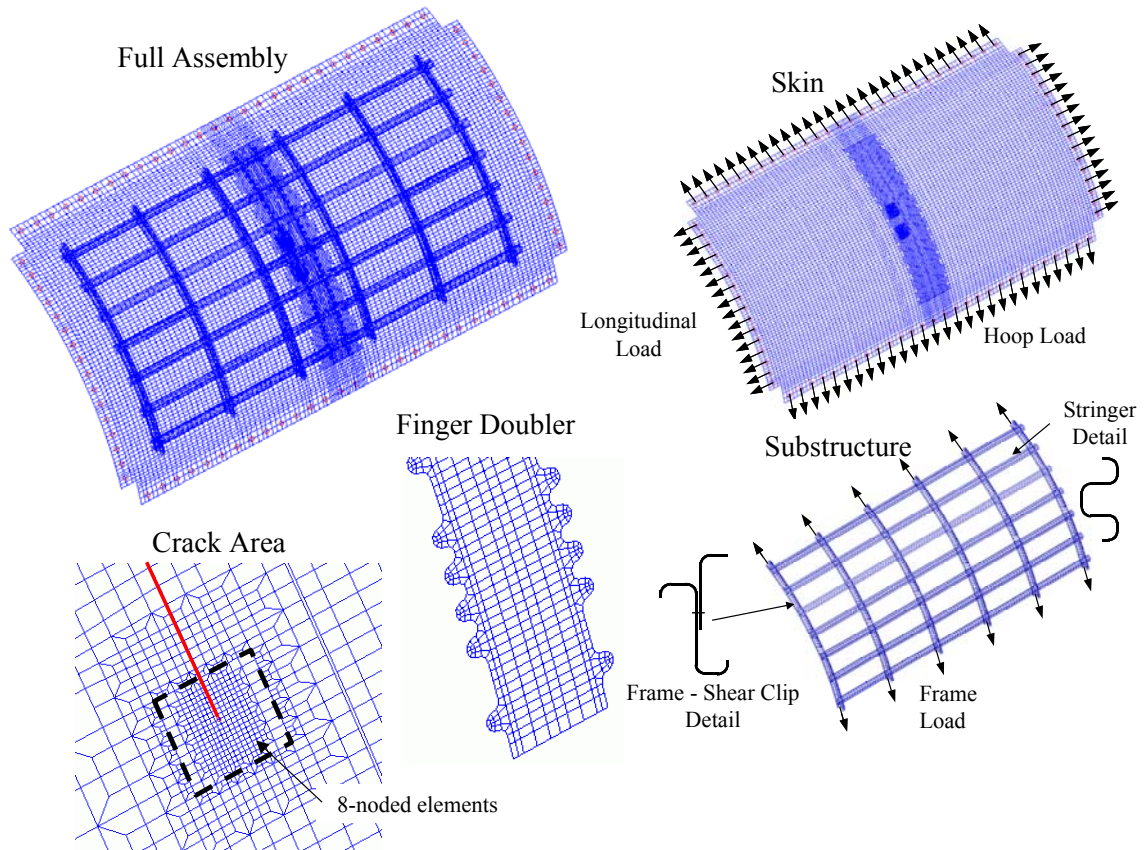


Figure 7. Finite element model of panel CVP3

The load conditions specified in Table 1 were simulated in the analysis. For the hoop, frame, and longitudinal loads, nodal point forces were applied at the load application points, as shown by the arrows in Figure 7. Internal pressure was applied to the inner surface of the skin.

The Modified Crack Closure Integral (MCCI) Method

In the MCCI approach [6-7], it is assumed that the energy released during crack extension is the same as the work that would be needed to close the crack and that the energy released can be related to the four components of SIF. The four components of SIF are the Mode I SIF caused by tensile load, K_I , the Mode II SIF caused by in-plane shear load, K_2 , the SIF due to symmetric bending loads, k_1 , and the SIF due to out-of-plane shear and twist loads, k_2 , as shown in Figure 8.

The MCCI method approximates the rate of work needed to close a crack using the local crack-tip displacements and forces. The displacements and forces at the nodes of the four elements surrounding the crack tip were obtained from the finite element results for each

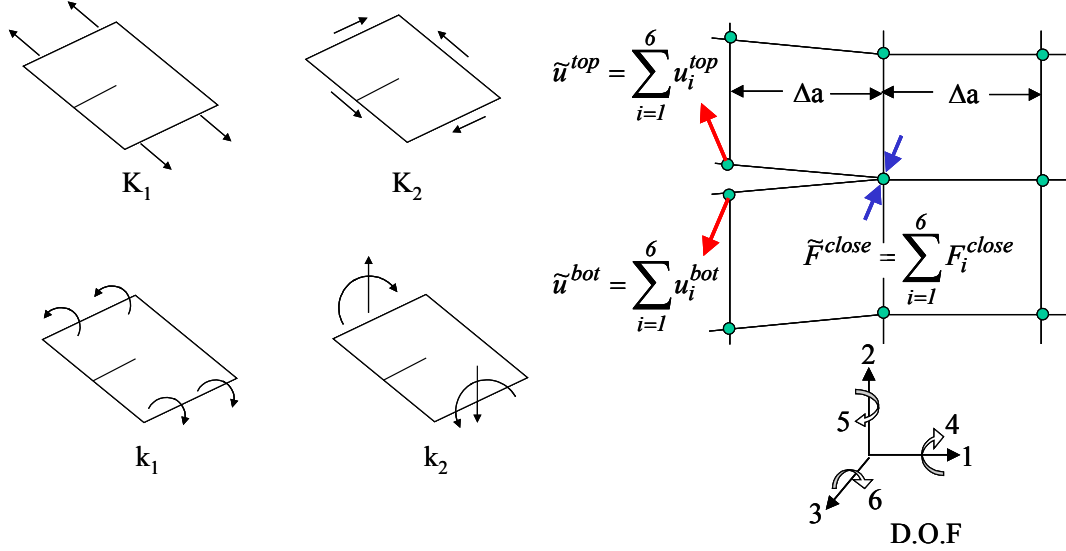


Figure 8. Definition of four stress-intensity factors and crack tip elements and nodes for computing the rate of work done to close a crack using the MCCI method

crack length, as shown in Figure 8. The work (W_i) done to close a crack of length Δa for each nodal degree-of-freedom (D.O.F) is given by [7]:

$$W_i = \frac{1}{2t\Delta a} [F_i^{Close} (u_i^{top} - u_i^{bot})], i = 1, \dots, 6 \quad (2)$$

where t is the thickness of the panel, F is the force needed to close the crack surfaces, u is the displacement component on each surface of the crack, and i denotes the D.O.F. The total amount of work done to close a crack of length Δa is numerically equal to the total amount of strain energy released during a crack growth increment of Δa , and the components of strain energy release rate can be related to the stress-intensity factors. Thus, the work done to close the crack is related to the SIFs as:

$$W_2 + W_6 = \frac{K_1^2}{E} \quad (3)$$

$$W_1 = \frac{K_2^2}{E} \quad (4)$$

$$W_4 = \frac{k_1^2 \pi}{3E} \left(\frac{1+\nu}{3+\nu} \right) \quad (5)$$

and

$$W_3 + W_5 = \frac{k_2^2 \pi}{3E} \left(\frac{1+\nu}{3+\nu} \right) \quad (6)$$

where, $E = 10500$ ksi and $\nu = 0.3$ are the Young's modulus and Poisson's ratio of the panel skin material and K_I , K_2 , k_1 , and k_2 are the SIF described earlier. Only the Mode I SIF, K_I , was used to predict the fatigue crack growth behavior because, as will be shown, it was found to be the dominant SIF.

RESULTS AND DISCUSSION

The effects of a lead crack and multiple cracking on the strain distribution and fatigue crack growth for both the longitudinal lap joint panels (CVP1 and CVP2) and the circumferential butt joint panels (CVP3 and CVP4) were studied in this project. Complete details are presented in reference 3. Key representative results are presented here.

Strain Distribution

The strain distribution was measured and predicted under quasi-static load conditions using the load components listed in Table 1 for the longitudinal lap joint and circumferential butt joint panels.

Longitudinal Lap Joint Configuration

The hoop strain in the skin at a mid-bay location is shown in Figure 9 as a function of applied pressure for panel CVP1 (lead crack only) and panel CVP2 (lead crack and multiple cracks). For each panel, the test was repeated twice using water and twice using

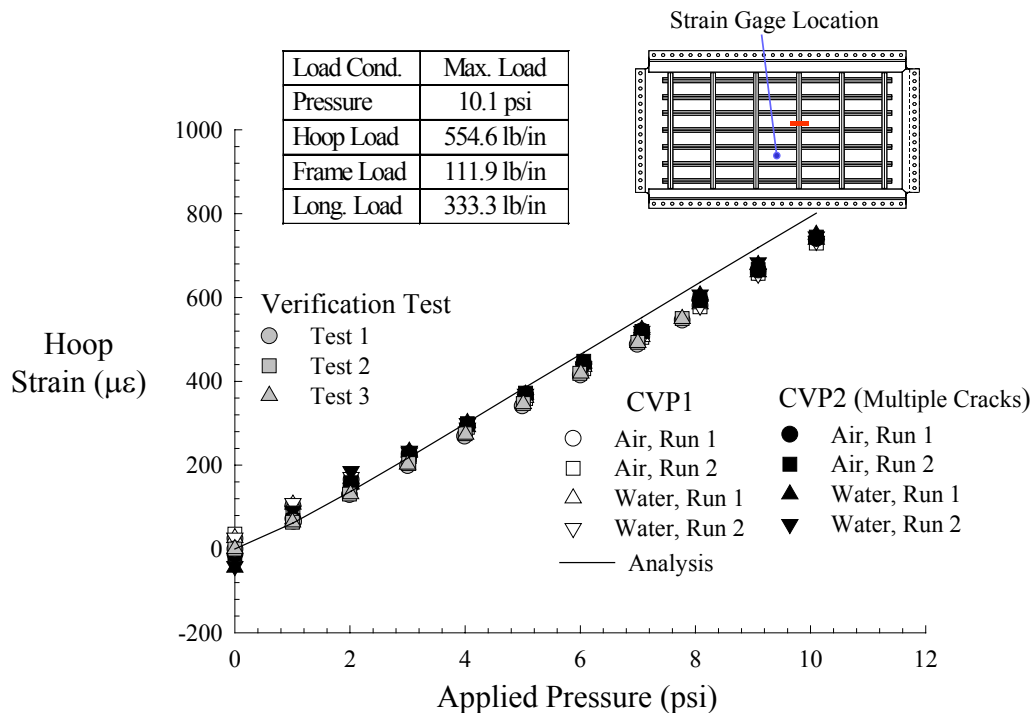


Figure 9. Hoop strain in panels CVP1 and CVP2 and in verification test

air to pressurize the panel. As shown in the figure, the strains are nearly identical for both panels for all four runs, indicating that the small multiple cracks have no effect on the global strain response at the given load levels. As expected, there were no differences in the results when air or water was used to pressurize the panel.

The strains from the full-scale verification test measured in the skin at a mid-bay location are also plotted in Figure 9. As shown in the figure, the results from panels CVP1 and CVP2 agree well with the full-scale verification test results for the given load levels. This indicates that the loading applied to panels CVP1 and CVP2 correctly simulates the pressurization of a fuselage section.

Also shown in Figure 9 is the finite element prediction using ABAQUS as described previously. The prediction, shown by the solid line in the figure, is in good agreement with the experimental data validating the finite element analysis.

The hoop strain in the skin for panels CVP1 and CVP2 is shown in Figure 10. The values shown for each panel are the averages of the four tests conducted. As shown in the figure, the magnitudes of the measured strains in both panels were similar and the distributions were nearly uniform across the middle of the panels. The multiple cracking did not effect the overall strain response.

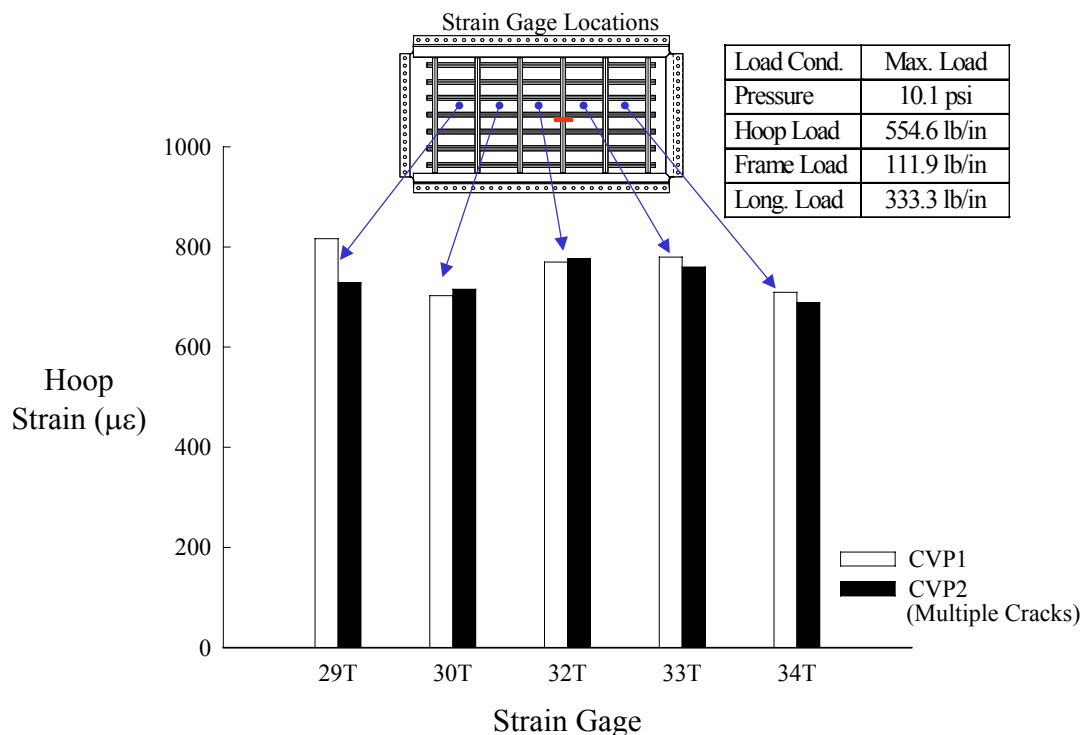


Figure 10. Hoop strain distribution in the skin mid-bay in panels CVP1 and CVP2

Circumferential Butt Joint Configuration

The longitudinal strain in the skin at a mid-bay location is shown in Figure 11 as a function of applied pressure for panel CVP3 (lead crack only) and panel CVP4 (lead crack and multiple cracks). The load was applied in ten equal increments up to the maximum values listed in Table 1 which simulates a fuselage down bend condition. For each panel,

the test was repeated twice using water and twice using air. As shown in the figure, the strains are nearly identical for both panels for all four runs indicating that small multiple cracks have no effect on the global strain response at the given load levels. As expected, there were no differences in the results when air or water was used to pressurize the panel. The prediction shown by the curve was in excellent agreement with experimental data.

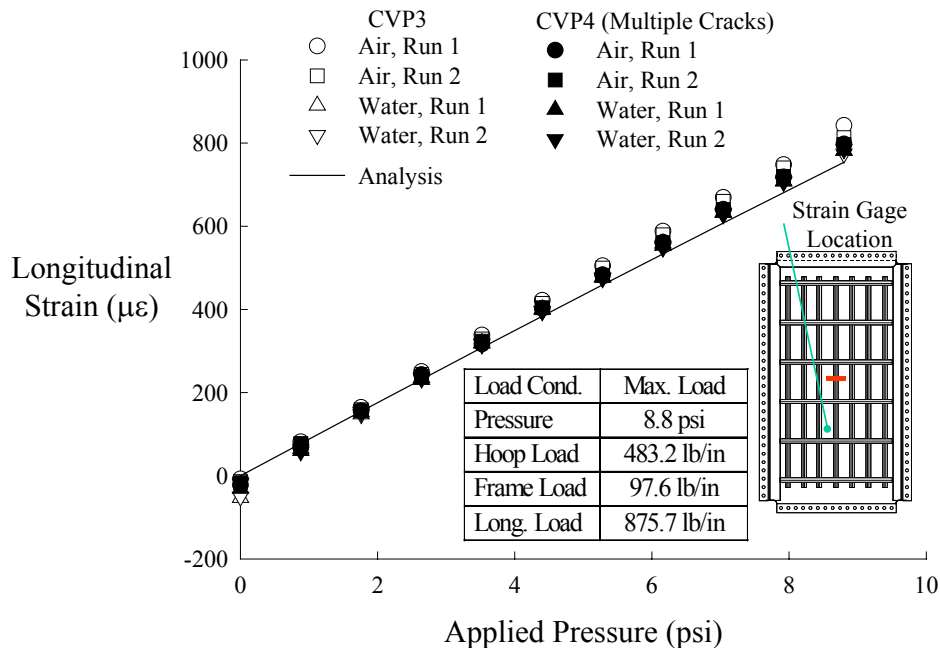


Figure 11. Longitudinal strain in skin at a mid-bay location in panels CVP3 and CVP4

In general, similar trends in strain gage data were obtained at the other gage locations in both joint configurations. That is, experimental results were very repeatable and the analytical predictions were in good agreement with the test results. Measured strains were nearly uniform in the middle of the panel. This provides confidence that the applied loads were introduced properly and the models have enough fidelity to capture the mechanical response. The small multiple cracks had no effect the global strain response.

Fatigue Crack Growth

The fatigue crack growth was measured in all panels under the constant amplitude loading using the maximum values of listed in Table 1. The growth of the lead crack and the multiple cracks was monitored and recorded. Representative results are presented for each joint configuration.

Longitudinal Lap Joint Configuration

Images of the crack extension under fatigue loading from the RCCM system are shown in Figures 12 and 13 for panels CVP1 and CVP2, respectively. The images show the progression of the damage from the original slit to the first adjacent rivet (3R and 3L). The block size of the grid paper on the top of each image is 0.05". In general, for both panels, the crack extension was symmetric and collinear indicating a symmetric load in the region of the crack tip. There was some out-of-plane (bulging) deflection of the crack face opposite the lap joint along stringer S4. There was little deformation of the crack face reinforced by the lap joint.

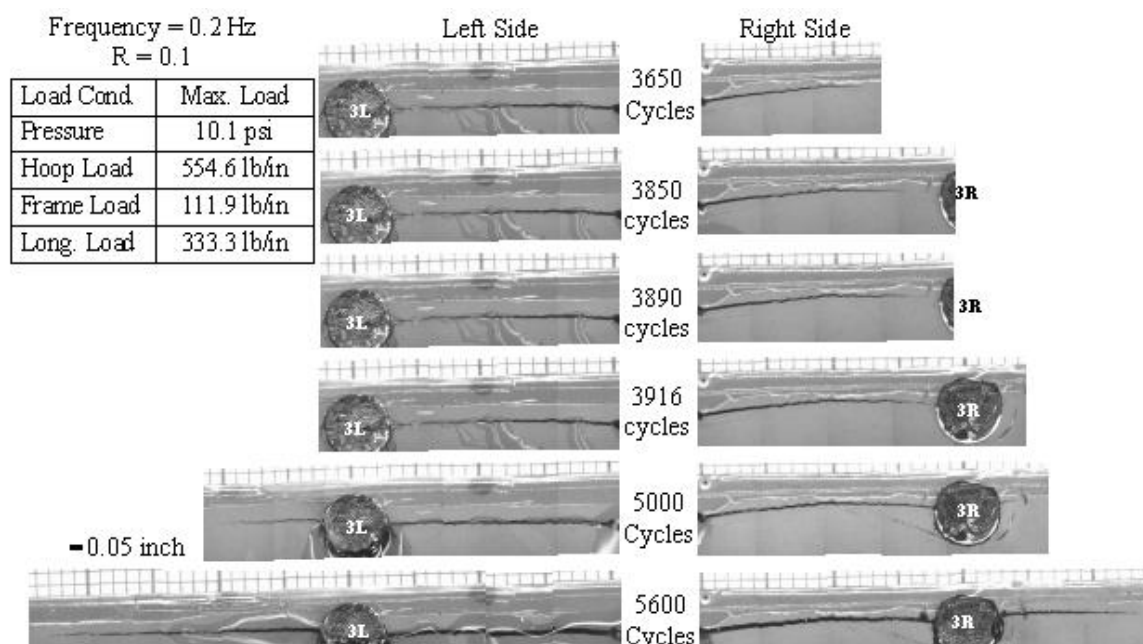


Figure 12. Images of crack growth in panel CVP1 during fatigue loading

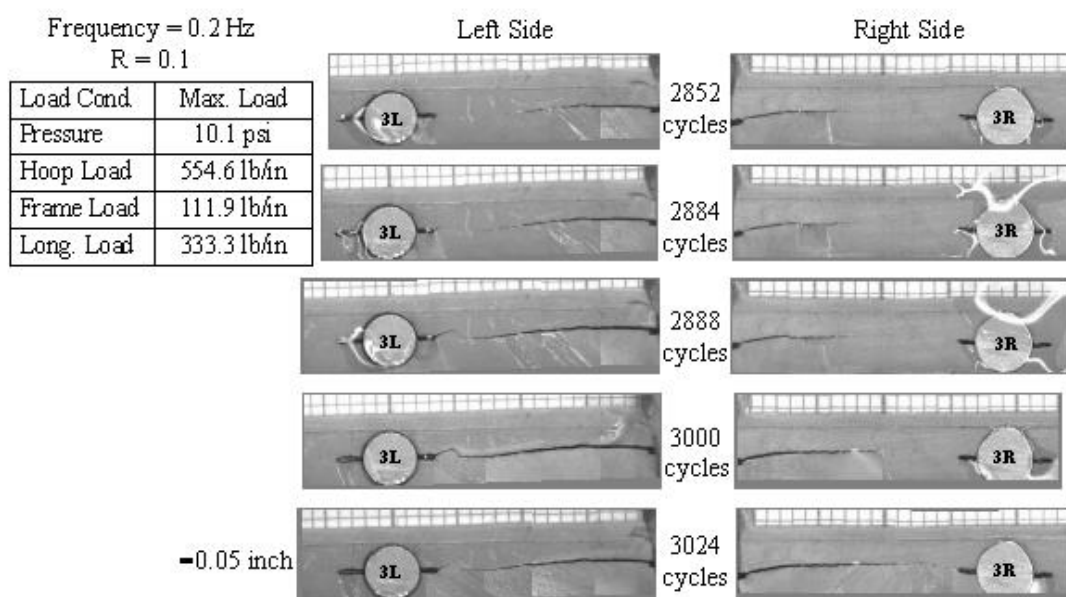


Figure 13. Images of crack growth in panel CVP2 during fatigue loading

The predicted stress-intensity factor ranges for the lead crack in panels CVP1 and CVP2 are shown in Figure 14. The numbers inside the circles along the x axis represent the location of rivets. As shown in the figure, ΔK_1 , which governs Mode I crack growth is the dominant SIF range. The next highest SIF range, ΔK_2 , which would cause Mode III crack growth, was not significant. Thus, only the Mode I SIF was used to predict the crack growth. As the lead crack tip approached the rivet directly ahead, the SIF increased more for CVP2 compared to CVP1 due to the small cracks at the rivet hole.

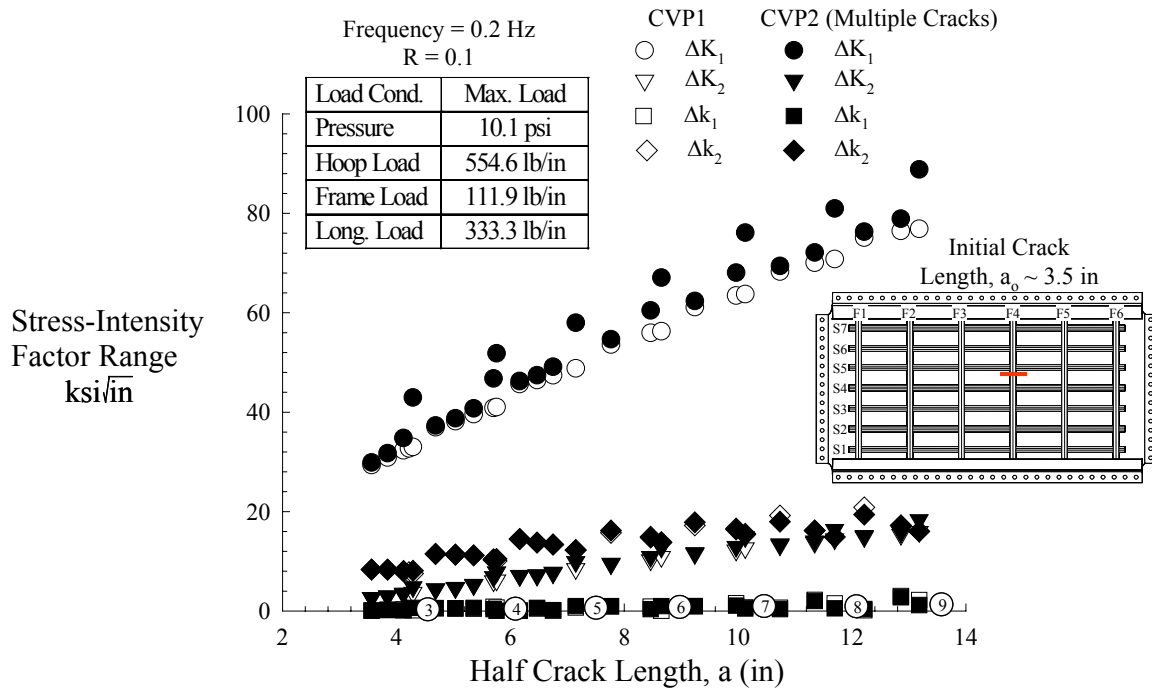


Figure 14. Stress-intensity factor range for panels CVP1 and CVP2

The half-length of the lead crack, as a function of number of fatigue cycles, is shown in Figure 15 for panels CVP1 and CVP2. The initial half-crack length prior to loading was 3.5". In the figure, the circular and square symbols represent the measured crack lengths at the left and the right crack tips, respectively, for each panel. The numbers inside the circles along the y axis represent the location of rivets. For panel CVP1, indicated by the open symbols, the vertical jumps indicate crack extension across a rivet hole when the crack length increased instantaneously by the diameter of the rivet hole. The rate of crack growth increased as the crack tip approached the rivet hole. The horizontal segments shown in the plot indicate the number of cycles before the crack reformed on the opposite side of the rivet hole. As the crack length increased, the delay in crack reformation (incubation period) decreased due to the larger crack driving force. For panel CVP2, which contained multiple cracks, the vertical jumps in the experimental data indicate linkup of the lead crack and a small multiple crack, when the crack length increased instantaneously by the diameter of the rivet hole plus the lengths of the small cracks at that rivet. There was no crack reformation required. As a result, the number of cycles needed to grow the lead crack to the final length (~12.5inches) in panel CVP2 was approximately 37% less than that in panel CVP1.

The Mode I SIF range, ΔK_I , (Figure 14) and crack growth data for 2024-T3 aluminum [8-10] were used in a cycle-by-cycle crack growth analysis program to predict the fatigue crack growth in panels CVP1 and CVP2, also shown in Figure 15. For panel CVP1, crack growth across rivet hole, indicated by the vertical jumps in the curve, was modeled by instantaneously increasing the length of the crack by the diameter of the rivet hole when the lead crack reached the rivet. For panel CVP2, crack growth at the rivet was modeled by instantaneously increasing the length of the crack by the diameter of the rivet plus the length of the small cracks at the rivet when the lead crack reached the first small crack. It

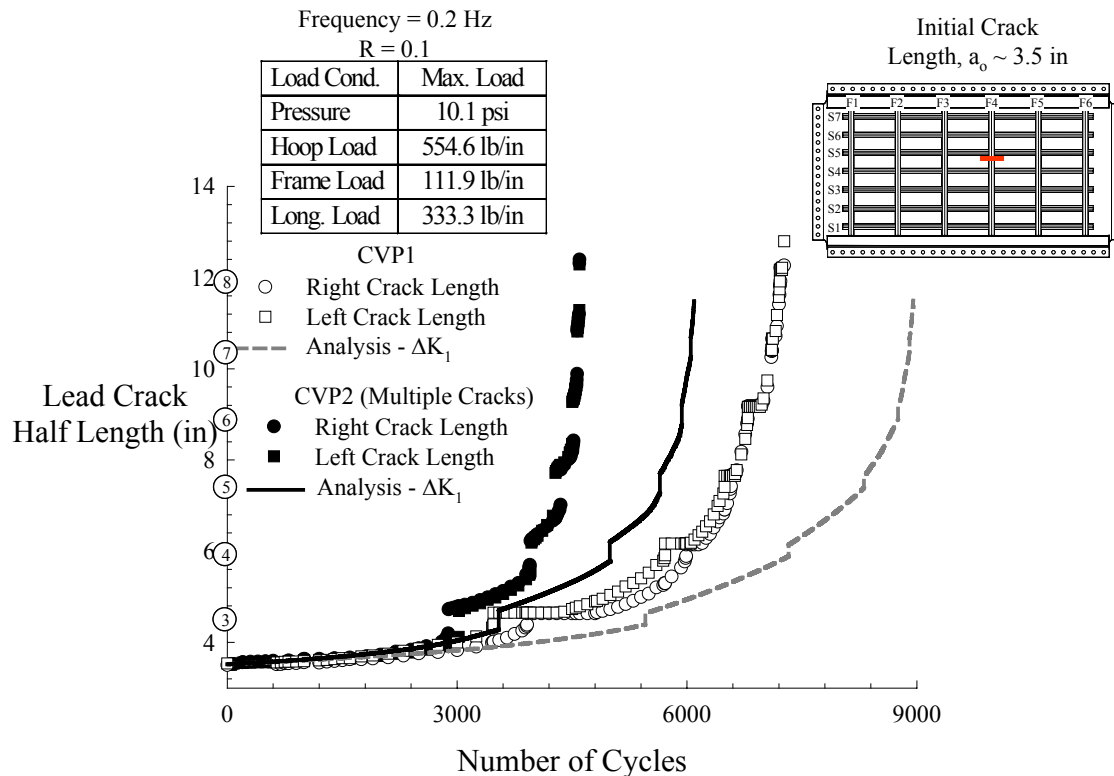


Figure 15. Half-crack length under fatigue loading for panels CVP1 and CVP2

is important to note that only ΔK_I was used to predict crack growth since it was the dominant SIF. The Δk_2 values shown in Figure 14 and the crack bulging observed during the test indicate some mode III loading. Mode III crack growth was not included in the crack growth analysis since the mode I component was the dominant component and there was no mode III experimental crack growth data. Good agreement was obtained between experiments and predictions relying on ΔK_I . For CVP2, the growth of the small multiple crack in the rivet ahead of the lead crack was not modeled in the analysis.

Circumferential Butt Joint Configuration

Images of the crack extension under fatigue loading from the RCCM system are shown in Figures 16 and 17 for panels CVP3 and CVP4, respectively. The images show the progression of damage from the original slit to the first adjacent rivet on either side (3R and 3L). The block size of the grid paper in each image is 0.05". For the circumferential butt joint panels, the crack paths meandered compared to those in the longitudinal lap joint panels shown previously in Figures 12 and 13. The crack growth of the lead crack and the small cracks at the first rivet ahead of the crack is shown in Figure 17 for panel CVP4. In general, it was observed that when the path of lead crack projected above or below the rivet directly ahead, the lead crack and the crack at the rivet grew past each other. This is shown in the images for the left crack tip in Figure 17. If the path of the lead crack intersected the rivet directly ahead, the crack tips coalesced as shown in the images for the right crack tip in Figure 17.

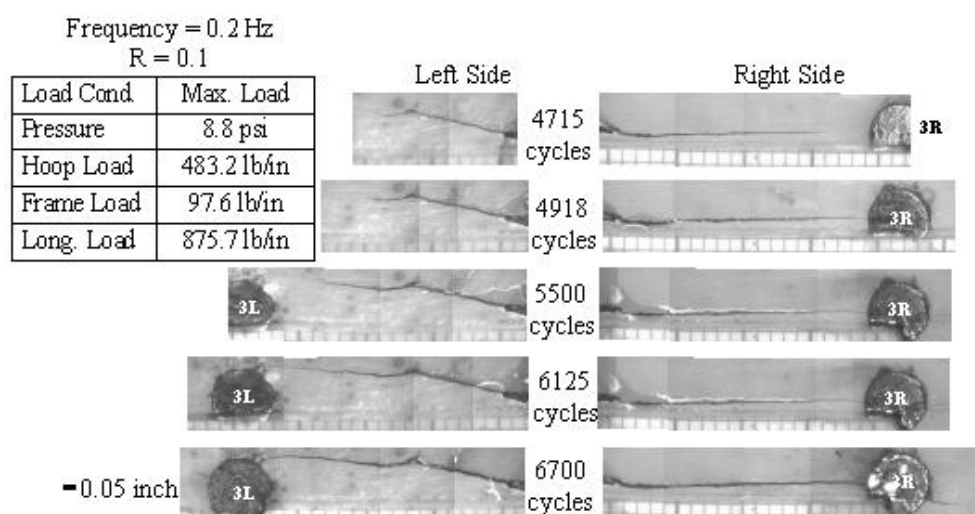


Figure 16. Images of crack growth in panel CVP3 during fatigue loading

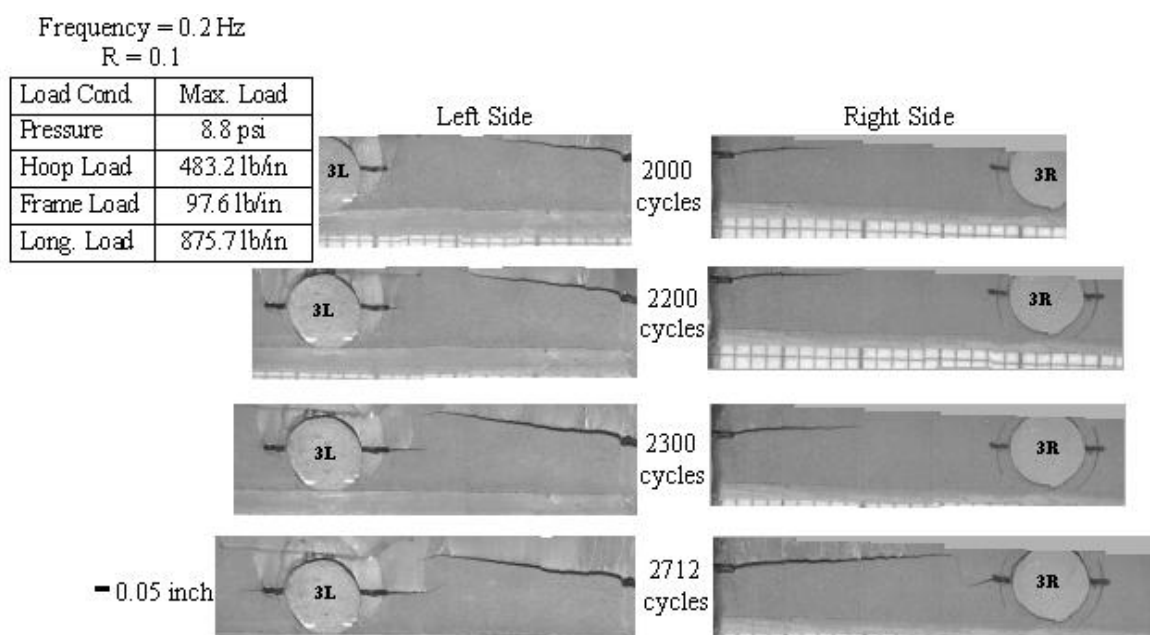


Figure 17. Images of crack growth in panel CVP4 during fatigue loading

The predicted stress-intensity factor ranges for the lead crack in panels CVP3 and CVP4 are shown in Figure 18. The numbers inside the circles along the x axis represent the location of rivets. As shown in the figure, ΔK_I , which governs Mode I crack growth, is the dominant SIF range. The next highest SIF ranges, Δk_1 and Δk_2 , which would cause crack-bulging deflections, were not significant. Thus, as for the longitudinal lap joint panels, only the Mode I SIF was used to predict the crack growth. As the lead crack tip approached the rivet directly ahead, the SIF increased more for CVP4 compared to CVP3 due to the small cracks at the rivet hole. In both panels, for crack lengths longer than the stringer spacing of 7.5", the SIF ranges decreased slightly due to the stiffening of stringers bridging the crack.

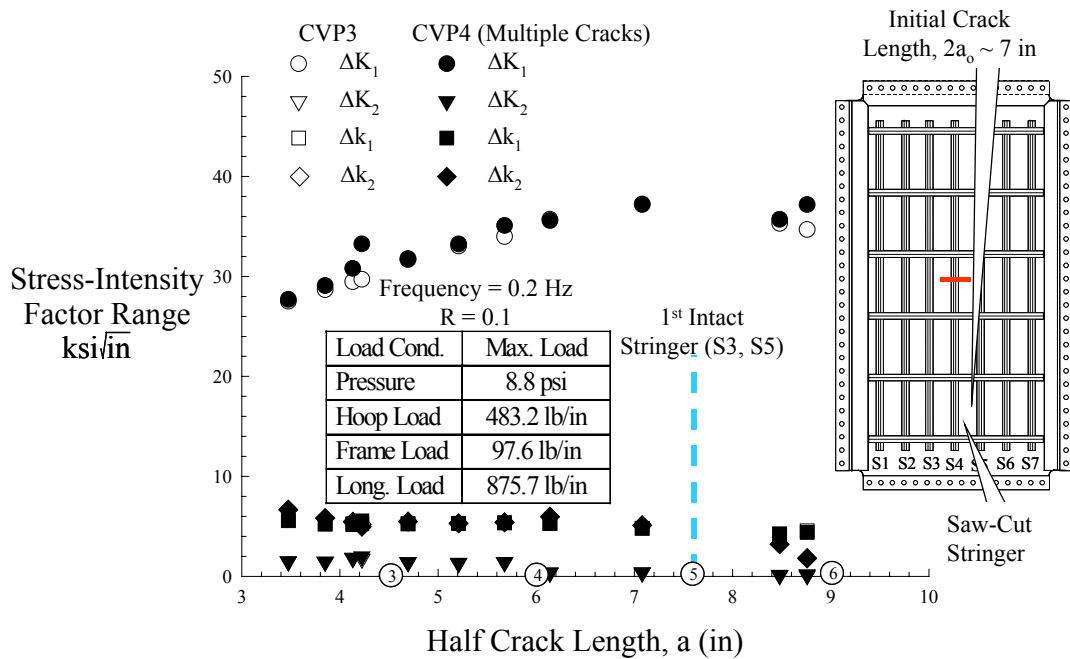


Figure 18. Stress-intensity factor ranges for panels CVP3 and CVP4

The fatigue crack growth behavior of panels CVP3 and CVP4 is shown in Figure 19. The initial half-crack length prior to loading was approximately 3.5". In the figure, the circular and square symbols represent the measured crack lengths of the left and the right crack tips, respectively, from both panels. The numbers inside the circles along the y axis indicate the locations of the rivets. For panel CVP3, crack growth across a rivet hole is indicated by a vertical jump in the data, where the crack length instantaneously increased

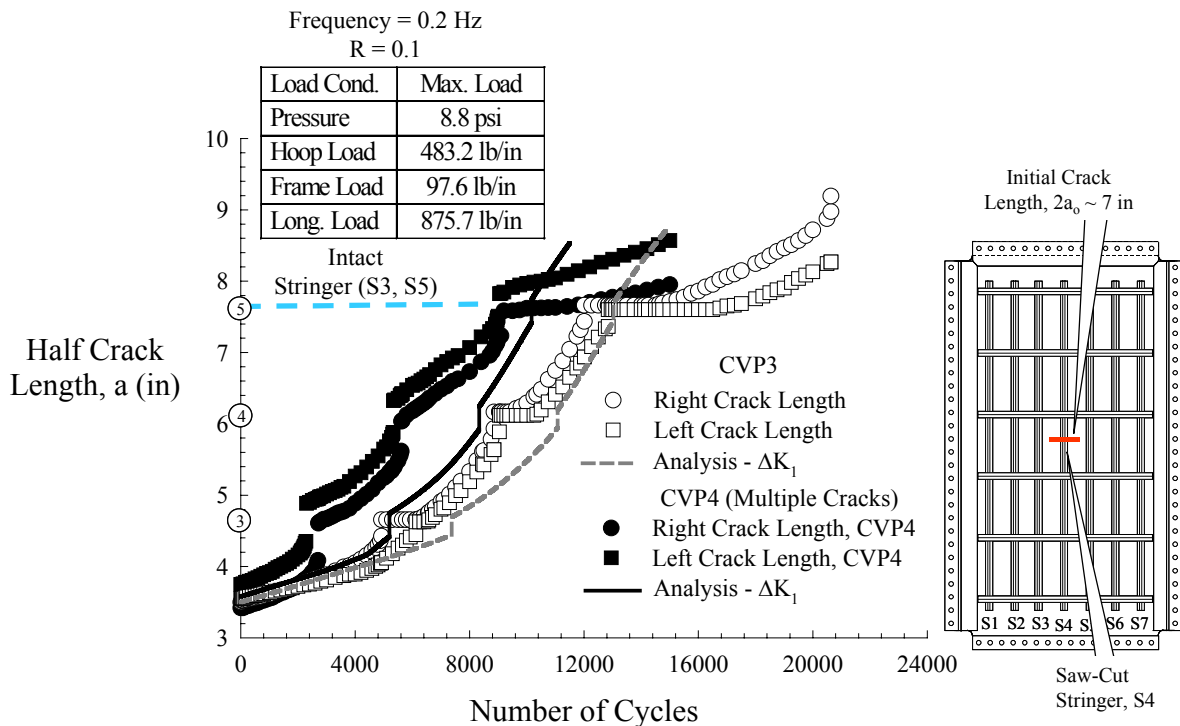


Figure 19. Half-crack length under fatigue loading for panels CVP3 and CVP4

by a length equal to the hole diameter. The horizontal segments shown in the plot indicate the incubation period or the number of cycles for the crack to reform on the opposite side of the rivet hole. For panel CVP4, which contained multiple cracks, the vertical jumps in the experimental data indicate the point when the lead crack and small multiple crack linked up. When this happened, the crack length increased instantaneously by the diameter of the rivet hole plus the lengths of the small cracks at that rivet. There was no crack reformation required. The small crack at the rivet hole on the opposite side became the new lead crack front. As a result, the number of cycles to grow the lead crack to the third rivet hole in panel CVP4 was approximately 27% less than that in panel CVP3. At the third rivet hole on either side, 5R and 5L, the crack had just reached the first intact stringers (S3 and S5). The additional stiffness added by the stringers increased the incubation period for panel CVP3 and decreased the subsequent crack growth rate for both panels.

The Mode I SIF range, ΔK_I , (Figure 18) and the crack growth data for 2024-T3 aluminum [8-10] were used in a cycle-by-cycle crack growth analysis program to predict the fatigue crack growth in panels CVP3 and CVP4, also shown in Figure 19. The analysis based on ΔK_I was in good agreement with the test data for crack growth in both panels until the crack reached the intact stringer. Little crack bulging was observed during the test, indicating that the crack growth was primarily due to Mode I loading.

CONCLUDING REMARKS

An experimental and analytical investigation was undertaken to assess the effects of small multiple cracks on the fatigue crack growth characteristics of curved panels with either a longitudinal lap splice or a circumferential butt joint. The Full-Scale Aircraft Structural Test Evaluation and Research (FASTER) facility was used to apply realistic loading conditions to curved panels representative of fuselage sections. Both quasi-static and constant amplitude fatigue loadings were applied to the panels. A geometrically nonlinear finite element analysis was used to determine the strain distribution in the panels and the fracture parameters necessary for predicting the fatigue crack growth behavior of the panel.

Four panels were tested, two panels with a longitudinal lap splice and two with a circumferential butt joint. For each joint configuration, one panel contained only a lead crack and the other contained a lead crack with small multiple cracks. Strains were measured under quasi-static loading conditions to ensure proper load introduction to the panels. The measured strains were repeatable and were in good agreement with the finite element analyses. The presence of multiple cracks did not affect the overall global strain response.

In general, symmetric, collinear crack propagation was observed under constant-amplitude fatigue loading for the four panels tested. Reasonable agreement was obtained between experimental fatigue crack growth data and predictions relying on the Mode I stress-intensity factors calculated using finite element analyses. The Mode I stress-intensity factor was the dominant component compared to the other modes. The number of cycles to grow a fatigue crack to a predetermined length was reduced by approximately 37% due to the presence of multiple cracks for the longitudinal lap joint panels and by 27% for the circumferential butt joint panels.

REFERENCES

1. Bakuckas, J. G., Jr., Bigelow, C. A., and Tan, P. W., "The FAA Full-Scale Aircraft Structural Test Evaluation and Research (FASTER) Facility," *Proceedings from the International Workshop on Technical Elements for Aviation Safety*, Tokyo, Japan, pp. 158-170, 1999.
2. Bakuckas, J. G., Jr., Akpan, E., Zhang, P., Bigelow, C. A., Tan, P. W., Awerbuch, J., Lau, A., and Tan, T. M., "Experimental and Analytical Assessments of Multiple-Site Cracking in Aircraft Fuselage Structure," *Proceedings of the 20th Symposium of the International Committee on Aeronautical Fatigue*, Seattle, Washington, USA, July 14-15, 1999.
3. Bakuckas, J. G. Jr., "Full-Scale Testing of Fuselage Structure Containing Multiple Cracks," *DOT/FAA/AR-01/46*, 2001.
4. ABAQUS Version 5.8, Hibbitt, Karlsson, and Sorensen (HKS), 1080 Main Street, Pawtucket, RI 02860, USA, 1998.
5. Swift, T., "Development of the Fail-Safe Design Features of the DC-10," *American Society for Testing and Materials Special Technical Publication 486*, 1970, pp. 164-214.
6. Rybicki, E. F. and Kanninen, M. F., "A Finite Element Calculation of Stress-Intensity Factors by a Modified Crack Closure Integral," *Engineering Fracture Mechanics*, Vol. 9, pp. 931-938, 1977.
7. Viz, M. J., Potyondy, D. O., and Zehnder, A. T., "Computation of Membrane and Bending Stress-Intensity factors for Thin, Cracked Plates," *International Journal of Fracture*, Vol. 72, pp. 21-38, 1995.
8. Hudson, C. M., "Effect of Stress Ratio on Fatigue Crack Growth in 7075-T6 and 2024-T3 Aluminum Alloy Specimens," *NASA TN D-5390*, 1969.
9. Phillips, E. P., "The Influence of Crack Closure on Fatigue Crack Growth Thresholds in 2024-T3 Aluminum Alloys," *ASTM STP 982*, pp. 505-515, 1988.
10. Dubensky, R. G., "Fatigue Crack Propagation in 2024-T3 and 7075-T6 Aluminum Alloys at High Stress," *NASA CR-1732*, 1971.